

# Synthesis of Carbon Nanotubes by Chemical Vapor Deposition (CVD).

A thesis submitted in partial fulfillment of the requirement  
for the degree of Bachelor of Arts with Honors in  
Physics from the College of William and Mary in Virginia,

by

William S M<sup>C</sup>Bride

Accepted for \_\_\_\_\_

(Honors, High Honors, or Highest Honors)

\_\_\_\_\_  
Advisor: Dr. Holloway

\_\_\_\_\_  
Dr. Bagdassarian

\_\_\_\_\_  
Dr. Griffioen

\_\_\_\_\_  
Dr. Kane

Williamsburg, Virginia

April 2001

## Abstract

The overall goal of this project was to analyze the data gathered from the study of nickel thin film versus catalyst particle size in order to build a predictive model for the synthesis of carbon nanotubes by chemical vapor deposition (CVD). Possible thermodynamic and kinetic processes involved in particle formation are discussed. It is catalyst particle size, which is dependant upon the initial thickness of the first row transition metal film, that is the key to controlling the multi-wall versus single-wall structure as well as the diameter of the nanotube when synthesizing carbon nanotubes by CVD.<sup>12</sup> Nickel thin films were sputtered at a power of 200 Watts for times of 100, 50, 25, and 15 seconds. The resulting nickel thicknesses of 13.0, 6.5, 3.3, and 2.0nm were annealed at 900<sup>0</sup>C for 3 minutes to achieve average particle sizes of 14.3±6.5, 4.4±1.9, 5.0±1.5, and 1.5±.5µm. The particle sizes were observed using scanning electron microscopy (SEM), and the average particle diameter data was used to build a predictive model with the form,  $y = (1040 \pm 115)x$  of nickel film thickness before annealing versus the catalyst particle size after a 3minute 900<sup>0</sup>C anneal.

## Introduction

There has been much interest in carbon nanotubes lately, especially for potential use in microelectronic devices.<sup>1</sup> The manner in which carbon forms bonds is the basis for the variety of carbon nanotube structures that are seen. An unbonded carbon atom has the electronic structure  $(1s)^2(2s)^2(2p)^2$ . In order to form covalent bonds one of the 2s electrons is promoted to 2p and the orbitals hybridize in one of three ways. The first is a hybridization of the 2s electron with one of the 2p electrons, forming two  $sp^1$  orbitals that are separated by an angle of  $180^\circ$ . This bond is linear and is the one in Acetylene,  $C_2H_2$ . The second is a hybridization of the 2s electron with two of the 2p electrons, forming three  $sp^2$  orbitals that are separated by  $120^\circ$  and are coplanar. This is the structure of graphite, which is comprised of bonds between the in-plane carbon atoms, which are arranged hexagonally. The in-plane bonding allows graphite to conduct electricity effectively along the planar axes.<sup>2</sup> In the third hybridization,  $sp^3$ , which results in the diamond structure, one 2s electron hybridizes with the three 2p orbitals and yields the characteristically tetrahedral  $sp^3$  bond. Crystalline diamond is thermodynamically metastable at room temperature and pressure, whereas graphite is the lowest energy state. This therefore allows the kinetic limits to be overcome and diamond to be converted to graphite at temperatures above  $1700^\circ C$  under normal pressures.<sup>2</sup>

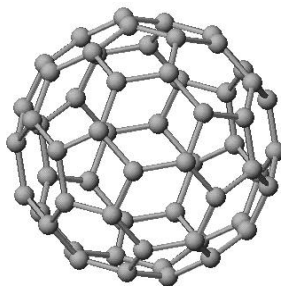


**FIG 1.**  $C_{60}$  Buckminsterfullerene. Primarily  $sp^2$  bond character.

The fullerenes, a group of spheroidal carbon molecules, show a blend of the  $sp^2$  and  $sp^3$  hybridization. The bond character of the fullerenes is primarily  $sp^2$ , with some  $sp^3$  shown in regions of high curvature.<sup>2</sup> The bonding in  $C_{60}$  is essentially  $sp^2$ , but there is some  $sp^3$  due to the curved surface of the isocohedron (see Figure 1). Nanotubes, like buckyballs, consist primarily of  $sp^2$ , but some  $sp^3$  character may be induced due to the presence of curvature, especially in the endcaps, or at kinks in the nanotube (see Figure 2).

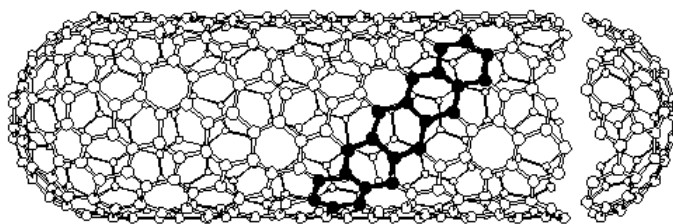


**FIG 2.** *Single-Walled Nanotube. Primarily  $sp^2$  bond character.*

Both single and multi-walled nanotubes may be synthesized, although I am primarily interested in the former. Multi-walled nanotubes (MWNTs) are essentially nested single-walled nanotubes of different diameters. Single-walled nanotubes (SWNTs) may be divided into three different categories, each of which is a pair of fullerene caps connected by a tube that is a rolled up seamless graphene sheet. The first of the three structural categories is zigzag, which is named for the pattern of hexagons as one moves circumferentially around the body of the tubule (Figure 3(a)). The second of these nanotube structures is termed armchair, which describes one of the two conformers of cyclohexane, a hexagon of carbon atoms, and describes the shape of the hexagons as one moves around the body of the tubule (Figure 3(b)). The third form is known as chiral (Figure 3(c)) and is believed to be the most commonly occurring SWNT. The name chiral means handedness and indicates that the tubes may twist in either direction.<sup>1</sup> The

geometry of the chiral SWNT lies between that of the armchair and zigzag SWNTs (see Figure 3(b)).

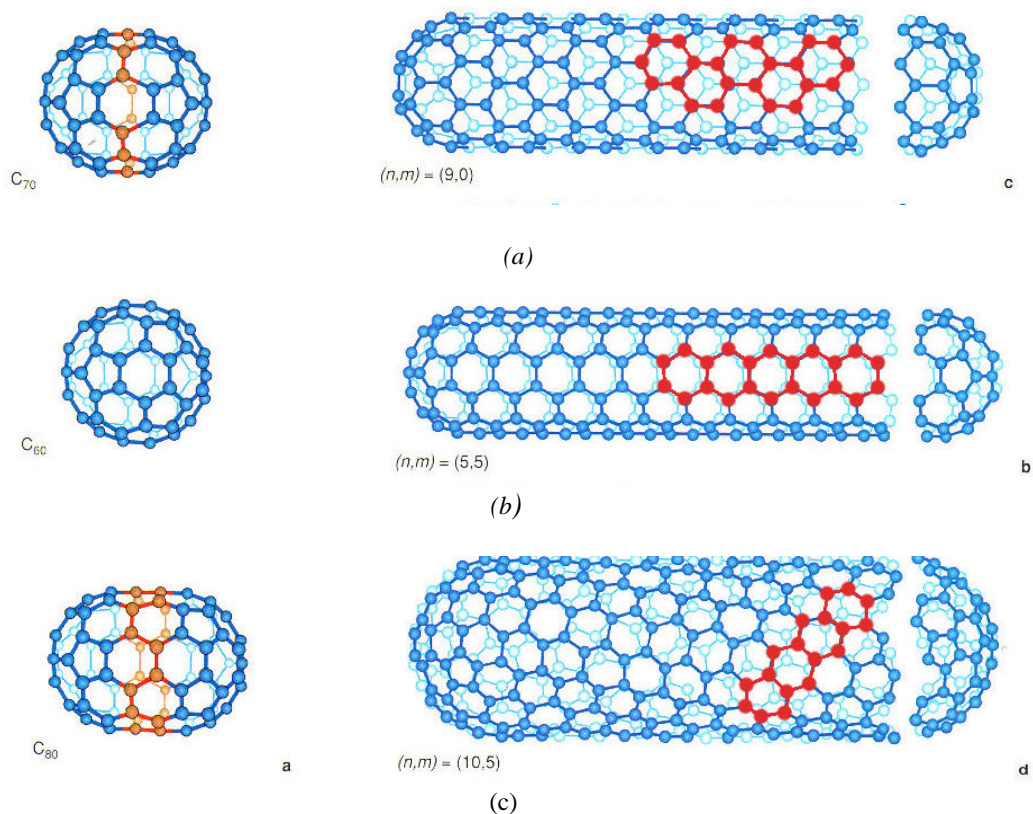


**FIG 3.** (a) Zig-Zag Single-Walled Nanotube. Note the zig-zag pattern around circumference and  $m = 0$ . (b) Chiral Single-Walled Nanotube. Note twisting of hexagons around tubule body. (c) Armchair Single-Walled Nanotube. Note the chair-like pattern around circumference and  $n = m$ .

The most straightforward manner in which to specify the structure of a tubule body is using a vector denoted  $\mathbf{C}$ , joining two equivalent points on the lattice.<sup>1</sup> The body of the tube is made by rolling up the flat graphitic sheet such that the two end points of the vector are superimposed.<sup>1</sup> Due to the high symmetry of the lattice many of the cylinders produced by this means are equivalent to one another. However, there is an "irreducible wedge" that is comprised of one-twelfth of the graphene sheet, within which unique structures are defined. Part of this is reproduced in Figure 4.<sup>2</sup>

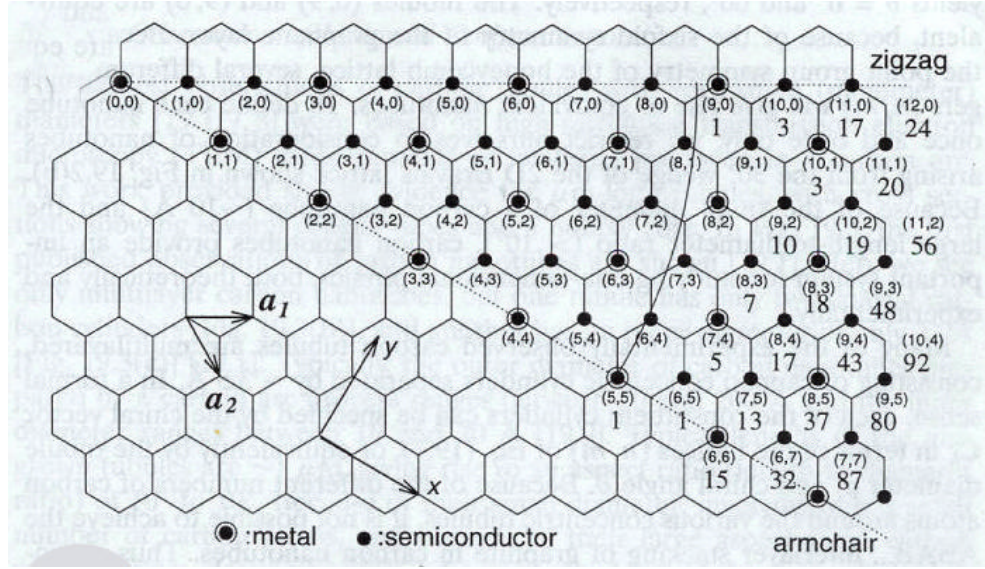


**FIG 4.** Possible vectors specified by the pairs of integers  $(n, m)$  for general carbon nanotubes, including armchair, zig-zag, and chiral. Below each pair of integers  $(n, m)$  is listed the number of distinct caps that can be joined continuously to the carbon tubule denoted by  $(n, m)$  as discussed in reference 2. The encircled dots denote metallic tubules while the small dots are for semiconducting tubules.<sup>2</sup>

Equation 1 defines the vector that describes, using Figure 4, the geometry of a SWNT. Vectors  $\mathbf{a}_1$  and  $\mathbf{a}_2$  are the unit cell base vectors of the graphene sheet, and  $n$  must be  $\geq m$ .

$$\mathbf{C} = n \cdot \mathbf{a}_1 + m \cdot \mathbf{a}_2 \quad (1)$$

It can be noted from Figure 4 that  $m$  is zero for all zigzag SWNT, and that  $n = m$  for all armchair nanotubes. All other SWNT's are chiral<sup>1</sup>. The chiral angle  $\theta$ , is defined as:

$$\theta = \sin^{-1} [m(3)^{1/2} / 2(n^2 + nm + m^2)^{1/2}] \quad (2)$$

If the chiral angle is zero one has an armchair tubule, if  $\theta = 30^\circ$  one has a zigzag tube. If  $0^\circ < \theta < 30^\circ$  then one has a chiral SWNT.

Nanotubes possess many fundamental properties that make them interesting and potentially useful. Nanotubes are extremely flexible, a SWNT can be bent into an arc with a radius of curvature as small as 20nm.<sup>2</sup> Nanotubes have an extremely high Young's

Modulus (1500–5000GPa).<sup>1</sup> SWNT's also possess remarkably high aspect ratios, 800-10<sup>4</sup>, the former being for a 0.9nm diameter tube and the latter for a greater than 100nm diameter vapor grown fiber.<sup>2</sup> Nanotubes also have notable electrical properties that are directly related to their unique quantum mechanical structure. All armchair SWNT's are metallic, and one-third of the possible chiral and zigzag tubes are metallic conductors. The remaining two-thirds of the chiral and zigzag tubes are semi-conductors (see Figure 4).

Examples of two uses for the unique properties of nanotubes are in carbon fiber composites, and microelectronics. Carbon fiber composites consist of a polymer matrix, within which are mixed whiskers of carbon fiber. Part of the reason that carbon fiber composites fall short of their theoretical strength limitations is due to imperfections in the carbon whiskers themselves.<sup>1</sup> If one used SWNTs in place of the traditional carbon whisker, that strength limitation would be eliminated. Furthermore, due to the extremely small (on the order of nanometers) diameter of SWNTs one could fabricate high-strength composite materials that are translucent in the visible range.

Another excellent use of nanotubes is in microelectronics. For example, a group of researchers at Harvard have built and demonstrated a SWNT bit. Calculations based on the device's small size suggest a density of up to 10<sup>12</sup> bits per square centimeter, and an operating frequency up to or even exceeding 100GHz. An added advantage is that the bit is non-volatile.<sup>10</sup>

There are three commonly used means by which to synthesize carbon nanotubes. Although all three are summarized here see Reference 1 for more information and process details for each method.

The first of these methods is laser ablation. A high power laser is rastered across a carbon target. In the plasma plume that is generated by the laser, provided that appropriate conditions exist, SWNTs form and are collected downstream from the plasma plume on a "cold finger".

The Arc-discharge method synthesizes nanotubes by using a fairly low voltage power supply to strike an electrical arc between two carbon electrodes. The carbon anode can be enriched with particles of a transition metal in order to aid synthesis. Nanotubes form in the arc and collect on the anode, along with a host of other carbon byproducts. The nanotubes that are synthesized by this means are typically very rosy and multi-walled.

Chemical vapor deposition (CVD) is the means of synthesis that is of interest for this study. CVD synthesis is achieved by taking a carbon species in the gas phase and using an energy source, such as a plasma or a resistively heated coil, to impart energy to a gaseous carbon molecule. Commonly used gaseous carbon sources include methane, carbon monoxide, and acetylene. The energy source is used to "crack" the molecule into a reactive radical species. These reactive species then diffuse down to the substrate, which is heated and coated in a catalyst (usually a first row transition metal such as Ni, Fe, or, Co) where it will bond. The result is that carbon nanotubes will form if the proper parameters are maintained. CVD allows the experimenter to avoid the process of separating nanotubes from the carbonaceous particulate that often accompanies the other two methods of synthesis. Excellent alignment,<sup>9</sup> as well as positional control on the nanometer scale,<sup>5</sup> can be achieved by the use of CVD. Control over the diameter, as well

as the growth rate of the nanotube can also be maintained.<sup>11</sup> The appropriate metal catalyst can preferentially grow single rather than multi-walled nanotubes.<sup>8</sup>

CVD carbon nanotube synthesis is essentially a two step process. A catalyst preparation step followed by actual synthesis of the nanotube. The catalyst particles must exist in order for one to grow carbon nanotubes by CVD. The catalyst is generally prepared by sputtering a transition metal onto a substrate and then using either a chemical etch or thermal annealing to induce catalyst particle nucleation. Ammonia may be used as the etchant. The thickness of the transition metal layer before the annealing step ranges from 1-200 nanometers.<sup>4, 5, 6, 9</sup>

Reported temperatures for the synthesis of nanotubes by CVD vary somewhat, but are generally within the 650-900°C range.<sup>4, 5, 6, 9, 11</sup> Common carbon sources are methane<sup>7</sup> and acetylene.<sup>5, 9</sup> Hydrogen must also be present during the synthetic step in order for nanotube synthesis.<sup>4, 5, 6, 9, 11</sup>

It has been shown that the size and material of the catalyst particles play a vital role during synthesis.<sup>11, 8</sup> I studied the formation mechanism of the catalyst particles in order to gain important insight into CVD nanotube synthesis.

## Experimental Methods:

Nickel thin films were deposited on 11mm<sup>2</sup> single crystal Silicon (Si) substrates that had been sequentially cleaned in a methanol and acetone wash and finally scrubbed in an ultrasonic bath. The vacuum chamber (the IBM chamber, see Figure 5) that was used to deposit the catalyst thin films has a base pressure of  $5 \cdot 10^{-6}$  Torr and is evacuated by means of a CTI Cryogenic Systems cryopump. Mass flow of the argon sputter gas was controlled by an MKS type 247 4-channel mass flow controller. The chamber was maintained at a pressure of  $5 \cdot 10^{-3}$  Torr during all sputtering runs . Sputtering was done at a power of 200 Watts on the Advanced Energy MDX-1k power supply connected to a US Guns Inc. MightyMak sputtering gun. Sputtering times of 100, 50, 25, and 15 seconds were chosen for this study. Thickness was measured sequentially to deposition *in-situ* using a Sycon Instruments STM-100 film thickness monitor. Nickel was used as the catalyst layer for all experiments.

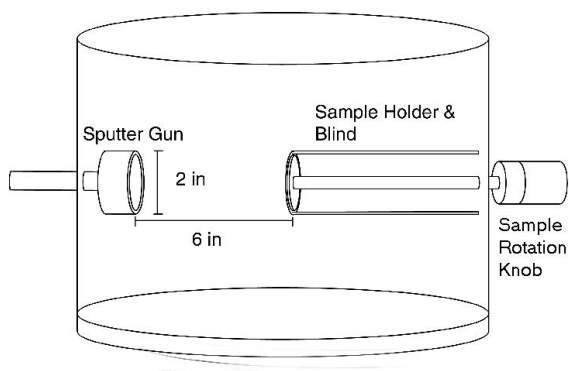


**FIG 5.** The IBM chamber. Sputtering chamber used to deposit all Ni thin films.

All annealing experiments were conducted in a separate growth chamber (the R2D2 chamber, Figure 6). The Ni coated Si substrates were annealed at 900<sup>0</sup>C for 3, 8, and 30 minutes. Colloidal graphite was used as an adhesive to affix a prepared substrate

onto the molybdenum (Mo) substrate heater. The R2D2 chamber also has a cooling system due to high operating temperatures. The cooling system consists of copper (Cu) tubing that is wrapped around the chamber near the rubber gaskets to stop them from degrading due to heat. The Gaskets on the R2D2 chamber are both Cu and Viton<sub>tm</sub>. The Cu gaskets are located at the thermocouple feedthrough, the mating of the chamber and both the Varian 524-2 cold cathode gauge and the Granville-Phillips convection gauge. The large top flange, bottom flange, and substrate heater flange are sealed by rubber gaskets. The R2D2 chamber has a base pressure of  $5 \times 10^{-6}$  Torr and is evacuated by a Veeco V-300 Dehydrator system equipped with a diffusion pump backed by a Welch piston actuated roughing pump. When being used to anneal the R2D2 chamber is at a minimum vacuum of  $5 \times 10^{-5}$  Torr. It should be noted that the pressure in the R2D2 chamber rises an order of magnitude at the beginning of annealing. While the heater coil is used to "crack" the carbon containing gas during growth, it is also used to radiatively heat our substrate during annealing. While annealing, the operational current is approximately 15 amperes through the tantalum (Ta) coil, and the power through the molybdenum (Mo) substrate heater reaches approximately 13 Watts. Prior to annealing experiments the "cracker" coil was carburized with acetylene to avoid Ta contamination of the substrates while annealing. The temperature of the substrate was measured with a k-type omega thermocouple, interfaced to a Fluke 51 II thermocouple reader. A higher annealing temperature of 1100<sup>0</sup>C was attempted but because it resulted in a significantly higher failure rate for the "cracker" coil these experiments were discontinued.

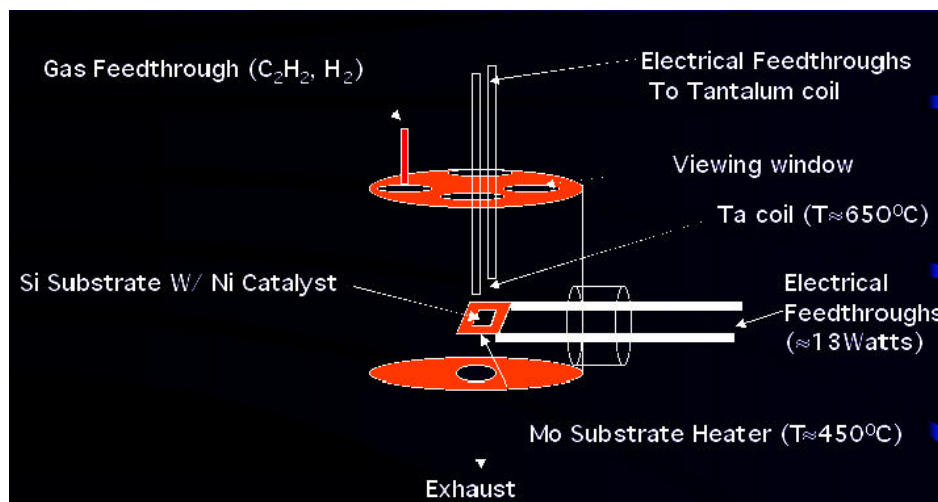


**FIG 6.** R2D2 Chamber . Annealing and synthesis chamber used to anneal all Ni thin films.

In order to try to resolve the surface features of the catalyst films two different microscopy methods were used during the course of this experiment. The scanning electron microscope (SEM) used was an Amray 1810 in backscatter mode with a 20kV electron beam. The Condenser Lens setting was typically 5-10 and is denoted within the black bar on each image. Typical magnifications used were between 1330-4020x and are denoted in the left hand corner of the black bar at the bottom of each image. The Metris atomic force microscope (AFM) was used in contact mode.

AFM was used in an effort to better quantify the particle size. Unfortunately, the AFM scans were at too high a magnification to show the micron-scale features that are more effectively seen in the SEM images that follow. The AFM was overly sensitive to the very steep walls of the Nickel particles. Because of this, tip breakage and image distortion both occurred during scanning. Ultimately, the SEM was used to gather all of the useful images for this experiment despite its lower resolution, largely because its resolution, while lower than that of AFM, was adequate to allow me to see the individual catalyst particles which were the focus of this work.

## **Results**

Figures 7 and 8 show SEM images for the Ni catalyst thin films. Recall that all sputtering was done at 200 Watts and all annealing as done at 900<sup>0</sup>C. The two parameters that I varied were the length of time of the sputtering (100, 50, 25, and 15 seconds) and the length of time of the annealing (3, 8, and 30 minutes).

I used a Sycon Instruments STM-100 IMF film thickness monitor (which is mounted in the substrate holder of the IBM chamber) to measure a Ni deposition rate at 200 Watts of 1.3 Angstroms/second allowing me to correlate sputtering time and thickness (see Table 1).

From Figure 7 it is obvious that particles of different sizes form after the different annealing times. I measured the diameter of particles from Figure 7 and tabulated them (see Table A1 in the appendix). The average particle diameters were calculated, as were the corresponding standard deviations (see Table 2).

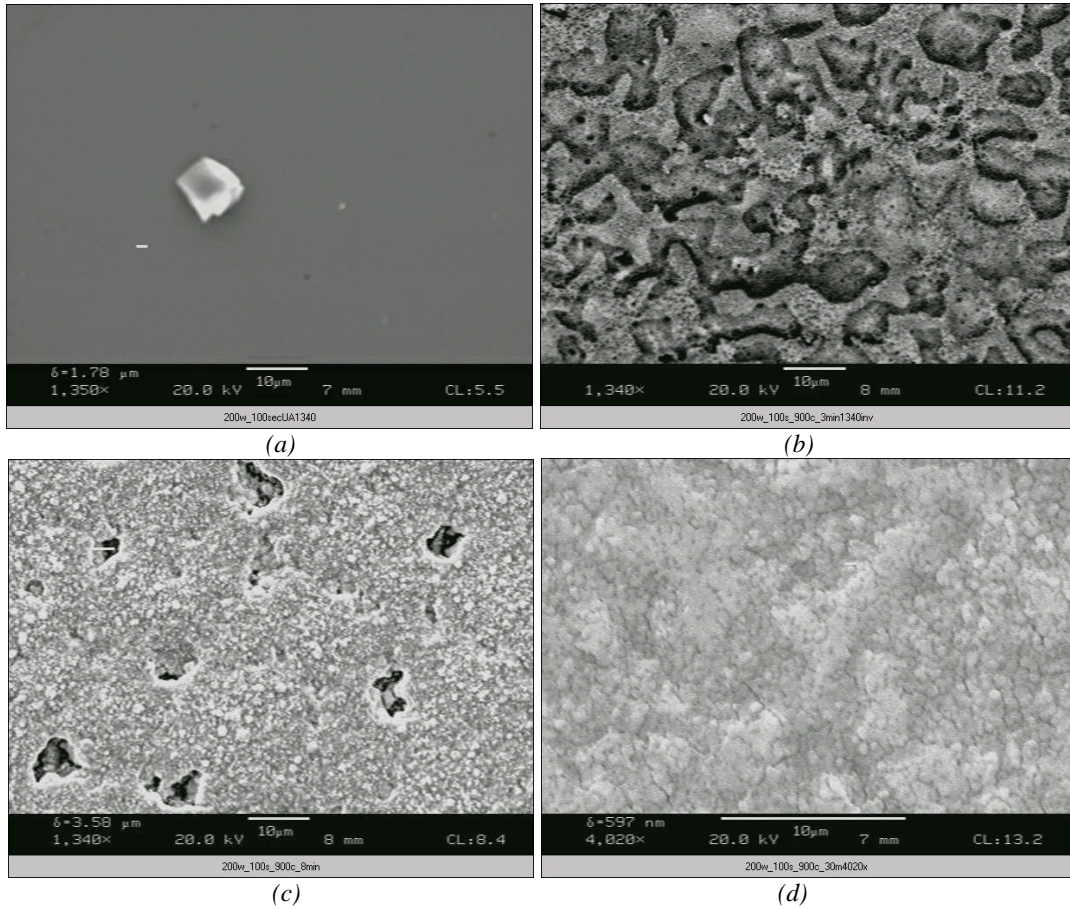


**FIG 7.** SEM images of 13 nanometer thick Ni film annealed at 900°C. Note 10 micron scale bar in each image. (a) The speck of dust is shown to give an idea of scale. The film is flat and featureless to the resolution of the SEM. Unannealed film. Magnification 1350x. (b) Rough feature size of 14.3 microns. Film annealed for 3min. Magnification 1340x. (c) Rough feature sizes present of 0.5 microns and 5 microns. Film annealed for 8min. Magnification 1350x. (d) Rough feature size of 600 nanometers. Film annealed for 30 min. Magnification 4020x.

100 second Ni film thickness (nm)	50 second Ni film thickness (nm)	25 second Ni film thickness (nm)	15 second Ni film thickness (nm)
13.0	6.5	3.3	2.0

\* Unless otherwise noted all reported values are  $\pm 1$  in the final digit reported

**Table 1** - Ni Film Thickness measured by Sycon Instruments STM-100 IMF film thickness monitor.

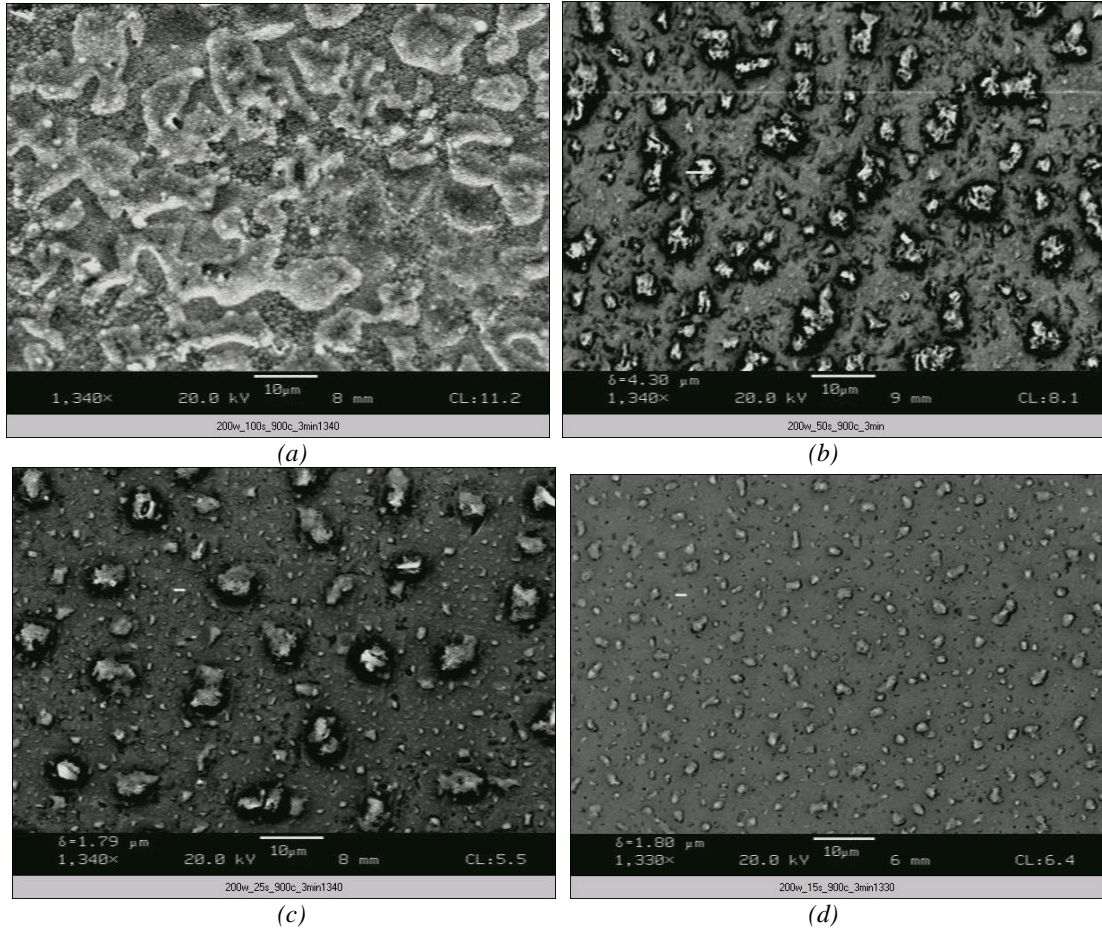


**FIG 8.** SEM images of Ni films annealed at 900<sup>o</sup>c. Note 10 micron scale bar in each image  
 (a) Feature size of  $14.3 \pm 6.5 \mu\text{m}$ . 13.0 nanometer Ni film annealed for 3 min. Magnification 1340x.  
 (b) Feature size of  $4.4 \pm 1.9 \mu\text{m}$ . 6.5 nanometer Ni film annealed for 3 min.. Magnification 1340x.  
 (c) Feature size of  $5.0 \pm 1.5 \mu\text{m}$ . 3.3 nanometer Ni film annealed for 3 min. Magnification 1340x.  
 (d) Feature size of  $1.5 \pm 0.5 \mu\text{m}$ . 2.0 nanometer Ni film annealed for 3 min. Magnification 1330x.

<b>100 second Ni film</b> <b>Ave. particle dia</b> <b>(<math>\mu\text{m}</math>)</b>	<b>50 second Ni film</b> <b>Ave. particle dia</b> <b>(<math>\mu\text{m}</math>)</b>	<b>25 second Ni film</b> <b>Ave. particle dia</b> <b>(<math>\mu\text{m}</math>)</b>	<b>15 second Ni film</b> <b>Ave. particle dia</b> <b>(<math>\mu\text{m}</math>)</b>
14.3±6.5	4.4 ±1.9	5.0±1.5	1.5±.5

**Table 2** - Average particle diameters and the corresponding standard deviation measured from Figure 8.

## Analysis and Discussion

Two trends from the above data will be the focus of this discussion. The first is for the samples with a 13.0 nm Ni film, the particles in the SEM images seem to get smaller and particle density increases (see Figure 7). The second pattern that I will discuss is that of decreasing particle size with decreasing thickness in the Ni films on the samples that were all annealed for 3 minutes (see Figure 8).

From an examination of Figure 7 there seem to be two processes occurring. The first is the nucleation of large distinct particles, which occurs within the first three minutes of annealing, this phenomenon may be seen in Figure 7(b). The second phenomenon is the seeming reduction of the large nuclei seeming to become many smaller nuclei with longer annealing times (see Figures 7(b), 7(c), and 7(d)).

In order to gain some insight into the particle nucleation mechanism the critical particle size was calculated neglecting surface terms and using the minimization of the equation<sup>13</sup> for the free energy of a spherical particle (Equation 3).

$$G = (4/3) \pi r^3 G_v + 4 \pi r^2 \gamma \quad (3)$$

$$G_v = -(kT/\Omega) \ln(P_v/P_s) \quad (4)$$

It should be noted that Equation 3 is for the solidification of a solid nucleus out of a super-saturated vapor, which is known as homogenous nucleation. Using this equation surface interaction effects are neglected but the results are still illustrative.

The  $G_v$  term (Equation 4) corresponds to the change in free chemical energy per unit volume of the particle. The  $\Omega$  contained in Equation 4 is the volume of an atom of Ni which is  $8.2 \cdot 10^{-30} \text{ m}^3$  and was calculated using the radius of an atom of Ni of 0.125 nm found in Reference 14.  $P_v$  is defined as the pressure of the supersaturated vapor ( $5 \cdot 10^{-7}$

Torr).  $P_s$  is defined as the pressure at the solid (Vapor Pressure Ni at  $924^{\circ}\text{C}$   $1 \cdot 10^{-8}$  Torr). The  $\sigma$  term is proportional to the free surface energy of the particle (see Equation 3). The  $\sigma$  value used in this analysis was  $1.9 \text{ J/m}^2$ .

When equation 3 is minimized and  $r^* = r$  ( $r^*$  being the minimum radius for particle nucleation to be energetically allowed), as well as  $dG/dr = 0$ , the critical nucleus size becomes:

$$r^* = -2\sigma / G_v \quad (5)$$

I calculated the critical radius for the nickel particles in the R2D2 chamber during annealing to be  $4.9 \cdot 10^{-10}$  meters. This is four orders of magnitude smaller than the particles that were observed (see Figure 7), which indicates that the nucleation process is not thermodynamically limited.

The possibility exists that there was a kinetic limit to particle nucleation during annealing. This was also considered and dismissed, at least in the case of the initial large particle formation, which is the process of interest. The large particle formation is of more interest due to the spacing of the particles. Figure 7 shows that the particles grow very large within a relatively short amount of time but the particle sizes shrink, and the density of the particles on the film increases with longer annealing times. If the amount of energy being put into the system was not sufficient for most atoms to reach the activation energy for nucleation, which would be true if the system were indeed kinetically limited, there would still exist some finite possibility that some particles would form and existing particles would grow after a 3 min anneal. However, if this were the case, then nuclei would form and their radius would steadily increase with annealing time. Provided that

this system is conservative (i.e. the amount of nickel on the sample is constant) the initial large particle formation process cannot be kinetically limited.

The vapor pressure of nickel is  $10^{-8}$  Torr at  $928^{\circ}\text{C}$ . The pressure within my chamber during annealing was approximately  $5 \cdot 10^{-5}$  Torr, and the mean free path of a gas atom at that pressure is approximately a meter. The R2D2 chamber has a diameter of 0.5 meters, which in conjunction with the fact that my chamber walls are much cooler than  $900^{\circ}\text{C}$ , makes it very likely that of the relatively small amount of nickel that evaporated from my film it would most likely either be evacuated by the pump, or be adsorbed by the wall of the R2D2 chamber. The smaller particles are therefore not the re-coalescence of evaporated nickel. These smaller particles must be forming from the larger, initially formed, particles. This process is much slower, possibly kinetically limited, and far less readily understood than the initial large particle formation. The extremely high particle density, which would tend to cause the synthesis of a more densely tangled mat of carbon nanotubes, made the longer annealing times less experimentally useful. Also, annealing a nickel film for 30 minutes is a less efficient use of chamber time and of less engineering interest. Therefore, the shorter 3 minute anneal time for the study of Nickel film thickness versus particle size after annealing was used.

It is catalyst particle size, which is dependant upon the initial thickness of the first row transition metal film, that is the key to controlling the multi-wall versus single-wall structure as well as the diameter of the nanotube when synthesizing carbon nanotubes by CVD.<sup>12</sup> The first step of the analysis was to perform some rudimentary calculations involving film thicknesses, average particle diameters, and measurements of particle density to verify that this is not only an approximately conservative system but

that the vast majority of the nickel in the original film is incorporated into nuclei. Using the values for average particle diameter from Table 2, I used the known area and thickness of the nickel to calculate what the average particle spacing should be (see Table 3). I deduced the empirical particle spacing by measuring the length and width of an area within an SEM image and counting the number of particles within that area. The theoretical particle spacing was calculated by using particle data from Table 2. I approximated this particle as a sphere and calculated its volume using the average particle diameter data. Using the known nickel film thicknesses (see Table 1) and the area of the substrate (  $1 \text{ cm}^2$ ) I calculated the volume of nickel present in each film. I then calculated the number of particles that would be present on the surface of that film. Using the fact that I knew the area of the substrate I deduced the theoretical spacing of the particles on the film. Note that the theoretical approximation is one order of magnitude larger than the experimentally derived values for the spacing of the particles. This is due in part because I am approximating low wide nickel features as spheres. If I merely treated each nickel particle as a hemisphere it would improve my estimated value by half an order of magnitude. Despite the rudimentary nature of my calculations the case can be made that this is a conservative system, at least to first approximation

-	13.0 nm Ni film Ave part spacing (m)	6.5 nm Ni film Ave part spacing (m)	3.3 nm Ni film Ave part spacing (m)	2.0 nm Ni film Ave part spacing (m)
<i>Exp</i>	2.4E-5	7.1E-6	1.2E-5	5.0E-6
<i>Theor</i>	3.4E-4	8.2E-5	1.4E-4	3.1E-5

\* Unless otherwise noted all reported values are  $\pm 1$  in the final digit reported

**Table 3** -Average particle spacing. Experimental values measured from Figure 8.

The average particle size against the film thickness is plotted in Figure 9. The data in Figure 9 follows a linear fit of each of the average particle diameter values. The

equation for the fit (see Equation 6) from Figure 9 was used to develop a predictive model for nickel film thickness versus nucleus size after a 3 minute anneal at 900°C. From this model both a table (see table 5) and a plot (see Figure 10) showing how thick a film I would need to anneal to get 10–100 nanometer particles. This is the ideal diameter range for single-walled carbon nanotube growth. Keep in mind that this is a continuum model, the validity of which is highest close to my known data points.

### Ni Film Thickness Vs Particle Size

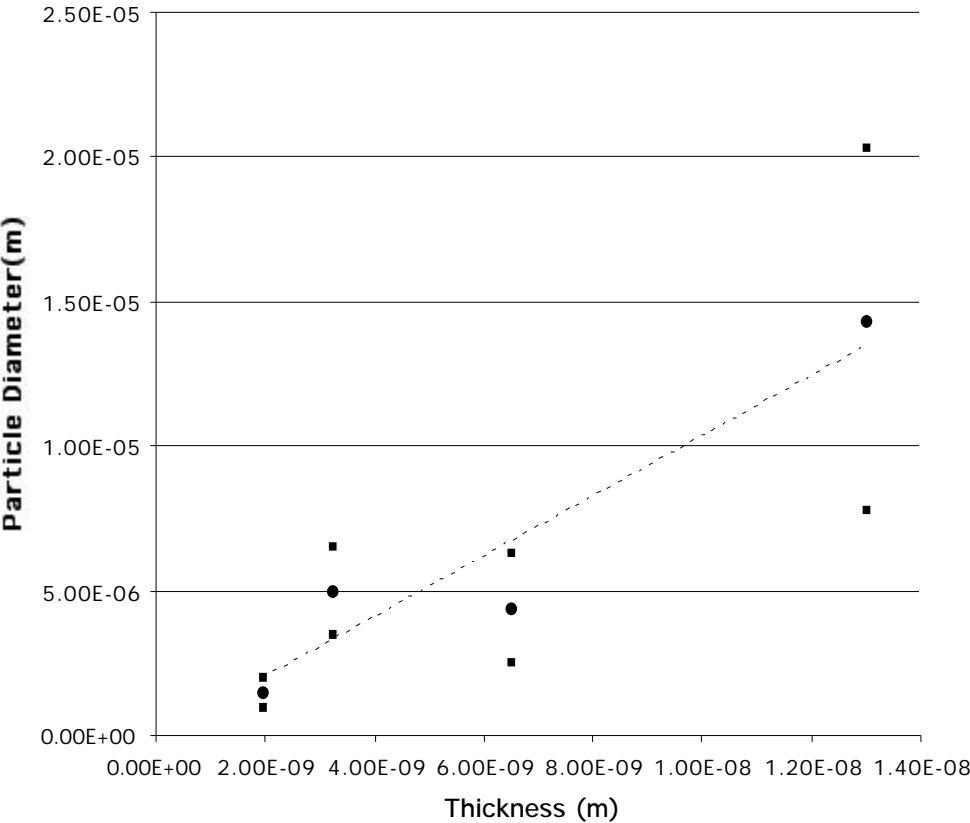


**FIG 9.** Nickel film thickness versus particle size. films annealed at 900°C for 3 minutes. Square points above and below the round points indicate standard deviation. Dashed line is an empirical best fit that is pinned at the origin.

$$y = (1040 \pm 115)x \tag{6}$$

The thickness of an atomic monolayer is 0.250 nm, the atomic diameter of a nickel atom<sup>14</sup>. In light of this the most plausible entry in Table 5 is the final entry when one considers the minimum thickness of a film of nickel. This model is a first-order approximation and needs refinement. This model is clearly valid only while the thickness of the sputtered Ni film is greater than the thickness of a monatomic layer of Ni.

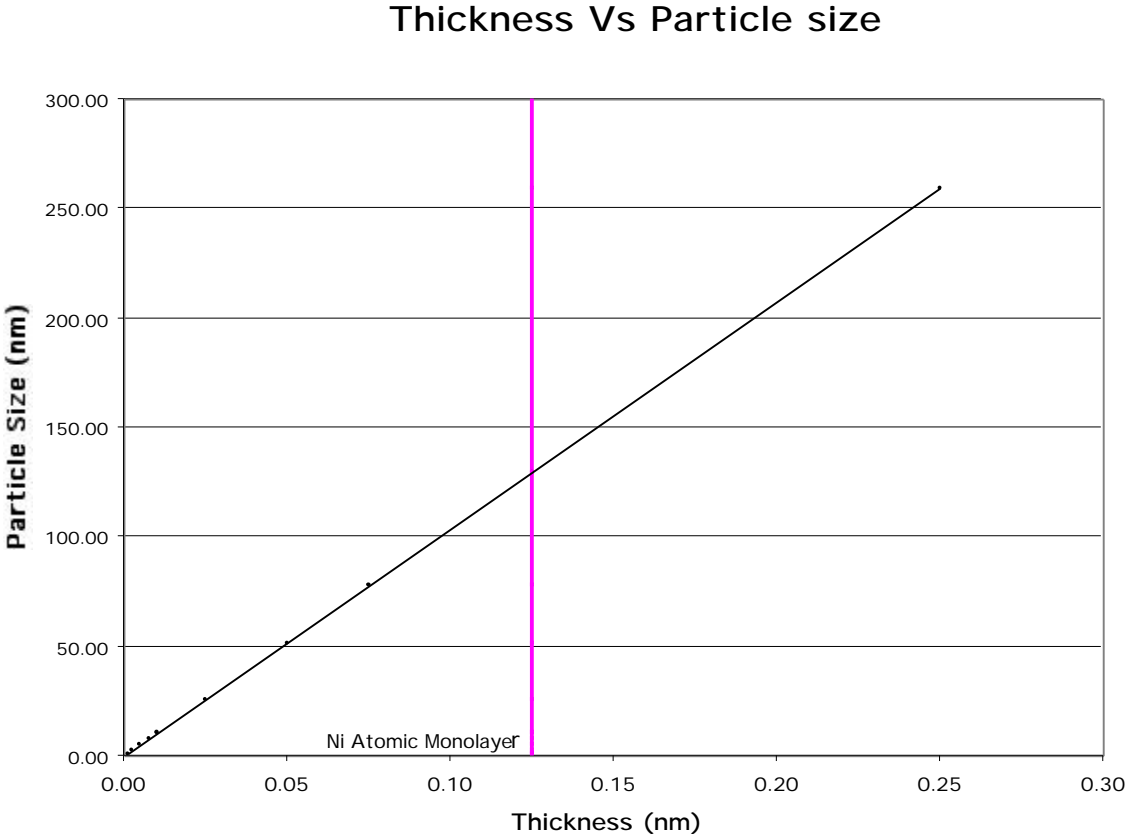


**FIG 10.** Thickness in nm versus particle size in nm for nickel film after 3min anneal at 900°C. This plot is developed from the best fit line from Fig 9 and correlates film thickness before annealing to particle size after annealing at 900°C for 3 minutes. Note that the red line indicates the thickness of an atomic monolayer of Ni.

Ni film thickness (m)	ave particle dia (m)
1.0E-12	1.0E-09
2.5E-12	2.6E-09
5.0E-12	5.2E-09
7.5E-12	7.8E-09
1.0E-11	1.0E-08
2.5E-11	2.6E-08
5.0E-11	5.2E-08
7.5E-11	7.8E-08
1.0E-10	1.0E-07

**Table 5** - Theoretical Ni film thickness to achieve ave particle diameter using 3 min 900 °C anneal.

## **Future Directions**

The next step in this research project is to examine the thickness of the films that are sputtered. The thickness needs to be reduced. This could be achieved by reducing the power of the sputtering gun to reduce the rate at which material is deposited, as well as building a chamber with a greater distance to the sputtering guns so that the sputtering rate could be reduced even further. Once these thinner Nickel films have been deposited and annealed I would conduct a further study to refine my theoretical model. I would then attempt to synthesize the carbon nanotubes by CVD.

In addition to synthesizing nanotubes I would suggest using novel catalyst deposition techniques to synthesize nanotubes in a grid-like distribution of clusters of single-walled nanotubes that are longitudinally aligned.

## References

- <sup>1</sup> P. J Harris, *Carbon Nanotubes and Related Structures*, Cambridge Press, (Cambridge, London, 1999)
- <sup>2</sup> M. S. Dresselhaus, G. Dresselhaus, and P. C. Ecklund, *Science of Fullerenes and Carbon Nanotubes*, AP, (New York, 1996)
- <sup>3</sup> H. O Pierson, *Handbook of Chemical Vapor Deposition*, Noyes, (Norwich, 1999)
- <sup>4</sup> M. Yudasaka, R. Kikuchi, T. Matsui, Y. Ohki, S. Yoshimura, and E. Ota, *Appl. Phys. Lett.* **67**, 17 (1995).
- <sup>5</sup> Z. F. Ren, Z. P. Huang, D. Z. Wang, J. G. Wen, J. W. Xu, J. H. Wang et al., *Appl. Phys. Lett.* **75**, 8 (1999).
- <sup>6</sup> M. Yukasaka, R. Kikuchi, Y. Ohki, E. Ota, and S. Yoshimura, *Appl. Phys. Lett.* **70**, 14 (1997).
- <sup>7</sup> C. J. Lee, D. W. Kim, T. J. Lee et al., *Appl. Phys. Lett.* **75**, 12 (1999).
- <sup>8</sup> S. B. Sinott, R. Andrews, D. Quian et al., *Chem. Phys. Lett.* **315**, (1999).
- <sup>9</sup> Z. F. Ren, Z. P. Huang, J. W. Xu, J. H. Wang et al., *Science.* **282**, 1105 (1998).
- <sup>10</sup> T. Reuckes, K. Kim, E. Joselevich et al., *Science* **289**, 94 (2000).
- <sup>11</sup> Y. C. Choi, Y. M. Shin, B. S. Lee, et al., *Appl. Phys. Lett.* **76**, 16 (2000).
- <sup>12</sup> Y. Y. Wei, Gyula Eres, V. I. Merkulov et al., *Appl. Phys. Lett.* **78**, 10 (2001).
- <sup>13</sup> M. Ohring, *The Materials Science of Thin Films*, AP, (New York, 1992)
- <sup>14</sup> J. Shackelford, *Materials Science For Engineers*, Prentice Hall, (New Jersey, 2000)

## **Acknowledgements**

### **Special thanks to :**

Professor Holloway, for guidance, patience and funding.

Professor Kane, for constant nanotube updates, and showing interest in this work.

Professor Griffioen, for emphasizing understanding, both personally and academically.

Professor Bagdassarian, for bringing zest to the chemistry department, and being a friend.

Jewel Thomas, for assistance with the SEM.

Amy Wilkerson, for assistance with the AFM.

Jason Gammon, for fielding literally thousands of questions.

Zhao Xin and Zeng Li, for assistance with catalyst.

Travis Turner, for the use of Figure 7

## Appendix

Particle Number	100 second Ni film particle dia (m)	50 second Ni film particle dia (m)	25 second Ni film particle dia (m)	15 second Ni film particle dia (m)
1	1.3E-05	4.0E-06	6.0E-06	1.8E-06
2	2.3E-05	4.6E-06	6.9E-06	1.3E-06
3	1.7E-05	2.5E-06	5.7E-06	1.4E-06
4	1.1E-05	3.6E-06	3.9E-06	8.7E-07
5	1.8E-05	3.4E-06	2.2E-06	7.4E-07
6	1.2E-05	3.4E-06	6.4E-06	1.6E-06
7	2.3E-05	6.2E-06	6.9E-06	2.0E-06
8	6.9E-06	7.0E-06	4.9E-06	1.2E-06
9	5.1E-06	5.2E-06	5.0E-06	2.4E-06
10	-	4.7E-06	6.8E-06	1.6E-06
11	-	1.9E-06	3.7E-06	9.2E-07
12	-	2.1E-06	5.7E-06	8.2E-07
13	-	2.3E-06	2.5E-06	2.0E-06
14	-	2.4E-06	7.0E-06	1.7E-06
15	-	4.4E-06	2.5E-06	1.1E-06
16	-	4.9E-06	4.0E-06	1.5E-06
17	-	6.9E-06	6.2E-06	2.2E-06
18	-	5.6E-06	4.7E-06	1.4E-06
19	-	6.6E-06	3.9E-06	1.9E-06
20	-	2.9E-06	5.5E-06	2.2E-06
21	-	3.4E-06	4.2E-06	1.5E-06
22	-	8.9E-06	-	-

\* unless otherwise noted all reported values are  $\pm 1$  in the final digit reported

*Table A1 -Particle Diameter. Measured from Figure 10*